Renewable and Sustainable Energy Reviews 40 (2014) 204–213

Contents lists available at ScienceDirect

Renewable and Sustainable Energy Reviews

journal homepage: www.elsevier.com/locate/rser

A stand-alone wind power supply with a Li-ion battery energy storage system

Tedjani Mesbahi [a,*], Ahmed Ouari [a], Tarak Ghennam [b], El Madjid Berkouk [c], Nassim Rizoug [d], Nadhir Mesbahi [a], Moudrik Meradji [b]

[a] Department of Electrical Engineering, Faculty of Sciences Engineering, Badji Mokhtar-Annaba University, P.O. Box 12, 23000 Annaba, Algeria
[b] Laboratoire d'Electronique de Puissance (LEP), UER: Electrotechnique, Ecole Militaire Polytechnique d'Alger, BP 17, Bordj EL Bahri, Alger, Algeria
[c] Laboratoire de Commande des Processus (LCP), Ecole Nationale Polytechnique d'Alger, BP 182, 10 Avenue Hassen Badi, 16200 el Harrach, Algeria
[d] Ecole Supérieure des Techniques Aéronautiques et de Construction Automobile, France

ARTICLE INFO

Article history:
Received 20 May 2013
Received in revised form
1 July 2014
Accepted 18 July 2014

Keywords:
Stand-alone power applications
Doubly fed induction generator
Li-ion battery
Back-to-back PWM converters
Permanent magnet synchronous machine and power management strategy

ABSTRACT

The improved structure of stand-alone wind power system which is presented in this paper based on a doubly fed induction generator (DFIG) and permanent magnet synchronous machine (PMSM). A Li-ion battery energy storage system is used to compensate the inherent power fluctuations (excess or shortage) and to regulate the overall system operation based on a power management strategy. The modeling and the control of a DFIG for stand-alone power applications are detailed. However, the magnitude and frequency of the DFIG stator output voltage are controlled under variable mechanical speed. This task is ensured via the control of *d* and *q* components of the rotor flux by means of a back-to-back pulse width modulation (PWM) converter connected to the rotor side of the DFIG. The PMSM is coupled mechanically to the wind turbine and supplies a required power to the PWM converter in order to regulate the dc bus voltage to the desired value.

In order to validate the proposed stand-alone wind power supply structure both a theoretical system analysis and a complete simulation of the overall wind energy conversion system (WECS) with Li-ion battery energy storage system is carried out to prove the performances of the control strategy.

Contents

* Corresponding author. Tel./fax: +21 338875398.
E-mail address: tedjani.mesbahi@estaca.fr (T. Mesbahi).

http://dx.doi.org/10.1016/j.rser.2014.07.180
1364-0321/

1. Introduction

Wind power and photovoltaic driven stand-alone systems have turned into one of the most promising ways to handle the electrification requirements of numerous isolated consumers worldwide [1]. These off-grid wind turbines or photovoltaic power systems help in reducing the stress on the grid, diminish the pollution and save on fuel cost by reducing or even eliminating the need for diesel generators, which consume a lot of polluting fuel [2,3]. Therefore, the implementation of stand-alone power systems can handle the rural electrification imbroglio effectively by providing environmentally benign, sustainable and reliable energy supply [4,5].

In recent years, the isolated grid and embedded applications (electric aircraft) used stand-alone wind power supply based on control of variable speed constant frequency (VSCF) generators has become a very important research topic [6–8]. However, many studies and evaluations about wind energy power potential were conducted in many European countries and America to develop wind energy power projects [9].

In this way, some stand-alone wind generation systems, where squirrel cage induction machine is used, are capable to regulate the output voltage magnitude but only at a variable frequency [4]. Others systems are able to achieve voltage magnitude and frequency regulation under variable speed thanks to the use of a PWM converter between the PMSM generator and the load [10]. Preceding from the last power wind architecture, Serra et al. [11] proposed a configuration consists of a rectifier followed by a dc/dc converter and a voltage source working as an inverter with an output filter. This wind power system is controlled in order to generate an output voltage with constant amplitude and frequency, irrespective of the supplied load.

Wang et al. [12] used in his study a hybrid wind-microturbine generation (MTG) distributed generation system that incorporates power electronic interfacing circuits for stand-alone operation.

Recently, the DFIG has been widely applied to wind energy conversion systems. The most important benefit of the DFIG is the small rate of power converter compared to the nominal power of machine (around 30%), so it can be used in high power applications in both grid and stand-alone mode [13].

In this context, the DFIGs are attracted attention as sources of constant frequency generators from variable speed movers [14,15]. In the rotor circuit, the speed range can be extended above synchronous speed and power can be generated both from the stator and the rotor. An advantage of this type of DFIG wind power is that can be operated under variable wind speed [15].

This paper presents an improved structure of stand-alone wind power system based on DFIG and PMSM. Nevertheless, the control strategy of our system developed for the purpose of regulating the rms value of the DFIG stator output voltage to 220 V and a nominal frequency at 50 Hz. The rotor of the DFIG is fed by both PMSM and Li-ion battery energy storage system via a PWM converter [16,17]. The control strategy of the DFIG uses a vector control scheme based on a d,q synchronous reference frame. The stator-flux vector is aligned with d-axis of the synchronous frame allowing by decoupled active and reactive powers control [15]. Two independent control loops are used; the first one is devoted to the stator voltage control while the second is dedicated to the rotor flux control. In a stand-alone wind power system the energy management strategy dispatches the power between the principal components of our system [7,18]. Many studies have been done on management strategies of wind energy conversion system [7]. Where, the authors propose a various management methods with different algorithms depend to the operating mode. For our case, a simple energy management strategy used to smooth wind power fluctuations by the Li-ion battery energy storage system.

The rest of this paper is organized as follows. The WECS system is briefly described in Section 2. The WECS model is discussed in Section 3. Section 4 presents the control of the WECS in isolated mode. Simulation results are presented in Section 5 to evaluate the proposed configuration and control. Finally, the conclusions are given in Section 6.

2. WECS description

Fig. 1 shows the simplified diagram of the power system based wind power generation in isolated mode. It consists of a wind turbine, a gearbox, a DFIG, a back-to-back PWM converter and a PMSM. Basically, the stator of the DFIG is directly connected to an isolated load where as its rotor is interfaced by a variable frequency power converter to cover a wide operation range from low to high power and assures the regulating of the stator voltage magnitude and constant frequency by controlling the rotor flux components [19]. The second PWM converter regulates the dc bus voltage by using the power generated from the PMSM [20].

3. WECS model

3.1. Modeling of the wind turbine and gearbox

The aerodynamic power P_{wind}, which is converted by a wind turbine, is related to the power coefficient C_p by the following equation [18,21,22]:

$$P_{wind} = \frac{1}{2} C_p(\lambda, \beta) \rho \, \pi \, R^2 V^3 \tag{1}$$

The wind turbine torque presents the ratio of the output power to the turbine speed Ω_t:

$$T_{aer} = \frac{P_{wind}}{\Omega_t} \tag{2}$$

The turbine is generally coupled to the generator through a gearbox whose gear ratio G is chosen somehow to set the generator shaft speed within a desired speed range. By neglecting the transmission losses, the torque T_g and shaft speed Ω_{mecref} to the generator side of the gearbox, are given by the following equation:

$$T_g = \frac{T_{aer}}{G} \text{ and } \Omega_t = \frac{\Omega_{mec}}{G} \tag{3}$$

A wind turbine can convert just certain percentage of the captured wind power. This percentage is represented by a coefficient $C_p(\lambda)$ that depends on the wind speed, turbine speed and

Nomenclature

P_{wind}	aerodynamic power
C_p	power coefficient
λ	tip speed ratio
ρ	air density
R	blade length
V	wind velocity
v_s, v_r	stator and rotor voltage vectors
i_s, i_r	stator and rotor current vectors
ϕ_s, ϕ_r	stator and rotor flux linkage vectors
ω_s, ω_r	stator and rotor angular frequency
M	mutual inductance
P_s, Q_s, P_r, Q_r	stator and rotor active and reactive powers
R_s, R_r	stator and rotor resistances
L_s, L_r	stator and rotor inductances
θ_s, θ_r	stator and rotor flux angles in the rotor frame
$v_{sd}, v_{sq}, v_{rd}, v_{rq}$	stator and rotor d,q voltages components
$i_{sd}, i_{sq}, i_{rd}, i_{rq}$	stator and rotor d,q currents components
$\phi_{sd}, \phi_{sq}, \phi_{rd}, \phi_{rq}$	stator and rotor d,q flux components
p	pole pairs number
T_{rm}	resistant torque
f	viscous coefficient
J	total inertia

pitch angle β.

$$C_p(\lambda,\beta) = (0.5 - 0.167(\beta-2))\sin\left[\frac{\pi(\lambda+0.1)}{10-0.3\beta}\right] - 0.00184(\lambda-3)(\beta-2) \tag{4}$$

C_p depends also to the ratio λ between the turbine angular velocity Ω_t and the wind speed. This ratio is called the tip speed ratio [14,18]:

$$\lambda = \frac{\Omega_t R}{V} \tag{5}$$

It is clear that the power extracted from the wind is maximized when C_p is maximized. This optimal value of C_p occurs at a defined value of the tip speed ratio λ. For each wind speed, there is an optimum rotor speed where maximum power is extracted from the wind [14,18]. For these reasons the turbine will often operate away from its maximum power point. By using the maximum power point tracker (MPPT) algorithm we can achieve the optimal operation of WECS. However, this algorithm allow to maximum the wind power conversion [18,22].

This algorithm can be summarized by five several steps, which are:

1. Choose the initial reference rotor speed and measure the output power of the generator.
2. Increase or decrease the reference rotor speed by one step (Ω_{step}) and measure the output power again.
3. Calculate $Sign(\Delta P)$ and $Sign(\Delta\Omega)$.
4. $\Omega_{mecref}(n) = \Omega_{mecref}(n-1) + Sign(\Delta P)Sign(\Delta\Omega)\Omega_{step}$.
5. Repeat from step 3 to reach optimum operating point.

3.2. General model of the DFIG

A classical modeling of the DFIG in the Park reference frame is used. The voltage and flux equations of the DFIG are given as follows [20,21,23]:

$$\begin{cases} v_{sd} = R_s i_{sd} + \frac{d\phi_{sd}}{dt} - \omega_s \phi_{sq} \\ v_{sq} = R_s i_{sq} + \frac{d\phi_{sq}}{dt} + \omega_s \phi_{sd} \\ v_{rd} = R_r i_{rd} + \frac{d\phi_{rd}}{dt} - \omega_r \phi_{rq} \\ v_{rq} = R_r i_{rq} + \frac{d\phi_{rq}}{dt} + \omega_r \phi_{rd} \end{cases} \tag{6}$$

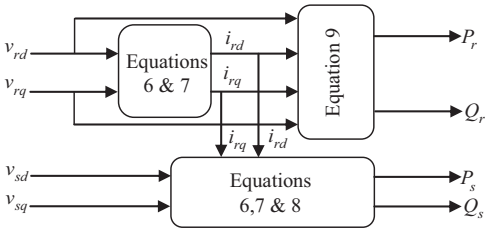

Fig. 2. General model of DFIG.

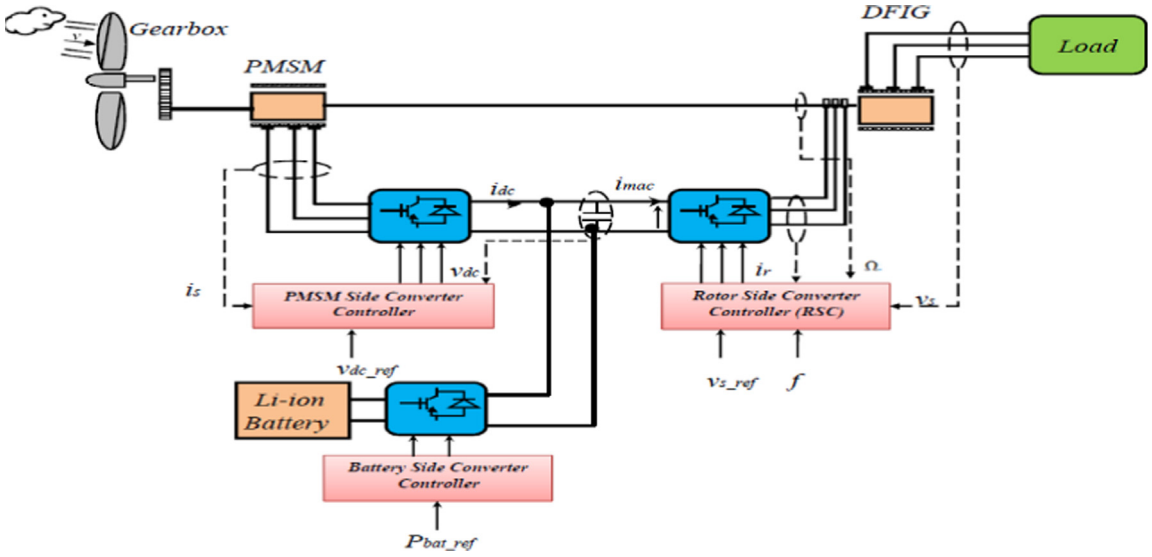

Fig. 1. Global configuration of the WECS.

with

$$\begin{cases} \phi_{sd} = L_s i_{sd} + M i_{rd} \\ \phi_{sq} = L_s i_{sq} + M i_{rq} \\ \phi_{rd} = L_r i_{rd} + M i_{sd} \\ \phi_{rq} = L_r i_{rq} + M i_{sq} \end{cases} \quad (7)$$

The active and reactive powers at the stator side and also at the rotor side are defined as follows:

$$\begin{cases} P_s = v_{sd} i_{sd} + v_{sq} i_{sq} \\ Q_s = v_{sq} i_{sd} - v_{sd} i_{sq} \end{cases} \quad (8)$$

$$\begin{cases} P_r = v_{rd} i_{rd} + v_{rq} i_{rq} \\ Q_r = v_{rq} i_{rd} - v_{rd} i_{rq} \end{cases} \quad (9)$$

Fig. 2 illustrates the block diagram of general model of DFIG. The electromagnetic torque is expressed as follows:

$$T_{em} = p(\phi_{sd} i_{sq} - \phi_{sq} i_{sd}) \quad (10)$$

The electro-mechanical torque equation is as follows:

$$T_{em} = T_{rm} + f\Omega + J\frac{d\Omega}{dt} \quad (11)$$

3.3. Modeling of the DFIG with a stator field orientation

Simplified expression of the electromagnetic torque is obtained by setting the following condition [19,23].

$$\begin{cases} \phi_{sq} = 0 \Rightarrow \frac{d\phi_{sq}}{dt} = 0 \\ \phi_{sd} = \phi_s \end{cases} \quad (12)$$

Hence, it yields:

$$T_{em} = p\phi_s i_{sq} \quad (13)$$

In consequence, the Park reference has to be synchronized with the stator flux (Fig. 3).

Assuming that the resistance of the stator winding R_s neglected, the voltage and flux equations of the stator windings can be simplified in steady state as follows:

$$\begin{cases} v_{sd} = 0 \\ v_{sq} = \omega_s \phi_s \end{cases} \quad (14)$$

$$\begin{cases} \phi_s = L_s i_{sd} + M i_{rd} \\ 0 = L_s i_{sq} + M i_{rq} \end{cases} \quad (15)$$

Since the DFIG stator voltage frequency is set by the control algorithm, the rotor speed is deduced from the following equation:

$$\omega_r = \omega_s - p\Omega \quad (16)$$

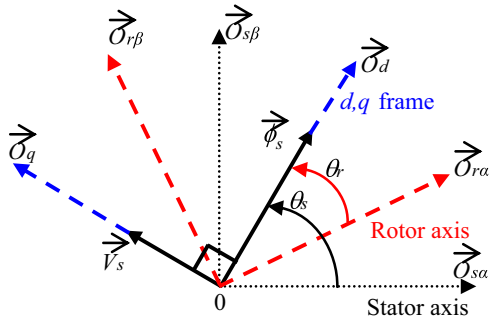

Fig. 3. Orientation of the *d*, *q* frame.

The angle θ_r is obtained by integrating the previous equation:

$$\theta_r = \int_0^t \omega_r dt + \theta_{r0} \quad (17)$$

From (15), the equations linking the stator currents to the rotor ones are deduced below:

$$\begin{cases} i_{sd} = \frac{\phi_s}{L_s} - \frac{M}{L_s} i_{rd} \\ i_{sq} = -\frac{M}{L_s} i_{rq} \end{cases} \quad (18)$$

The following constraint can be deduced from (7) and (18). It corresponds to the correct orientation of the reference frame.

$$i_{rq} = -\frac{L_s}{M} i_{sq} \Leftrightarrow \phi_{rq} = \frac{\sigma L_s L_r}{M} i_{sq} \quad (19)$$

From (8), (14) and (19) the stator active and reactive powers become:

$$\begin{cases} P_s = \frac{(1-\sigma)}{\sigma M}\sqrt{3}\, v_s \phi_{rq} \\ Q_s = \frac{(1-\sigma)}{\sigma M}\left(\sqrt{3}\, v_s \phi_{rd} - \frac{L_r}{M}\frac{3}{\omega_s} v_s^2\right) \end{cases} \quad (20)$$

Consequently, the control of stator active power is ensured by a *q* rotor flux component control ϕ_{rq} while the control of stator reactive power is guaranteed by *d* rotor flux component control ϕ_{rd}.

3.4. Modeling of the DFIG in isolated mode

In this case the DFIG model consists of the following equations which link the rotor flux with the rotor voltages [8–16]:

$$\begin{cases} \frac{d\phi_{rd}}{dt} = -\frac{\phi_{rd}}{T_r} + v_{rd} + E_d \\ \frac{d\phi_{rq}}{dt} = -\frac{\phi_{rq}}{T_r} + v_{rq} + E_q \end{cases} \quad (21)$$

with:

$$\begin{cases} E_d = \frac{M}{T_r} i_{sd} + \omega_r \phi_{rq} \\ E_q = \frac{M}{T_r} i_{sq} - \omega_r \phi_{rd} \end{cases} \quad (22)$$

The stator voltages equations are:

$$\begin{cases} v_{sd} = -\omega_s \frac{M}{L_r}(\phi_{rq} + A_d) \\ v_{sq} = +\omega_s \frac{M}{L_r}(\phi_{rd} + A_q) \end{cases} \quad (23)$$

with

$$\begin{cases} A_d = \frac{L_r}{M}(L_s \sigma\, i_{sq} - \frac{R_s}{\omega_s} i_{sd}) \\ A_q = \frac{L_r}{M}(L_s \sigma\, i_{sd} + \frac{R_s}{\omega_s} i_{sq}) \end{cases} \quad (24)$$

The block diagram showing model of the DFIG in this mode is illustrated in Fig. 4.

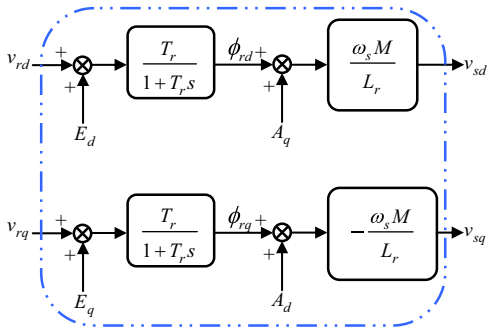

Fig. 4. DFIG model in isolated mode.

3.5. Modeling of the PMSM in isolated mode

The model of the PMSM in the (dq) is described by the following equations:

$$\begin{cases} v_{md} = R_{ms} i_{md} + L_d \frac{di_{md}}{dt} - E_{md} \\ v_{mq} = R_{ms} i_{mq} + L_q \frac{di_{mq}}{dt} - E_{mq} \end{cases} \quad (25)$$

where E_{md} and E_{mq} are the thermal coupling

$$\begin{cases} E_{md} = \omega L_q i_{mq} \\ E_{mq} = -\omega L_d i_{md} - \omega \phi_f \end{cases} \quad (26)$$

with

v_{md}, v_{mq}: The direct and quadrature voltage components.

i_{md}, i_{mq}: The direct and quadrature current components.

3.6. Equivalent continuous model of the converters

The dynamic of this wind generation system is slower than the switching frequency of power converters. Moreover, the high frequency of voltages and currents may be neglected due to the presence of the rotor windings and filter inductors, and the high commutation frequency used by PWM converters. Therefore, only the low frequency spectrum of the various quantities of the model requires to be calculated. An equivalent continuous model of the converter has been established with the voltage and current balancing condition. In the d,q reference frame, the rotor voltages are linked to the dc bus voltage v_{dc} and the equivalent d,q component control modulation signals ($m\,mac_{d\_reg}, m\,mac_{q\_reg}$) as [19,21,23] follows:

$$v_{rd} = m\,mac_{d\_reg} \frac{v_{dc}}{2} \quad (27)$$

$$v_{rq} = m\,mac_{q\_reg} \frac{v_{dc}}{2} \quad (28)$$

Similarly, for the PMSM side converter the relations between the equivalent d,q component control signals ($m\,m_{d\_reg}, m\,m_{q\_reg}$) and the d,q components of the actual voltages can be given as follows:

$$v_{md} = m\,m_{d\_reg} \frac{v_{dc}}{2} \quad (29)$$

$$v_{mq} = m\,m_{q\_reg} \frac{v_{dc}}{2} \quad (30)$$

The evolution of the dc voltage $v_{dc}$is given by the following equation:

$$C \frac{dv_{dc}}{dt} = i_{m\_mac} - i_{dc} \quad (31)$$

C is the total capacitor value of the dc-bus.

So, modulated currents are expressed by the following equation:

$$i_{dc} = \frac{1}{2}(m\,m_{d\_reg} i_{rd} + m\,m_{d\_reg} i_{rq}) \quad (32)$$

$$i_{mac} = \frac{1}{2}(m\,mac_{d\_reg} i_{rd} + m\,mac_{d\_reg} i_{rq}) \quad (33)$$

3.7. Electrical battery model

3.7.1. Batteries technologies

The batteries are made of stacked cells where-in chemical energy is converted to electrical energy and vice versa. The desired battery voltages as well as current levels are obtained by electrically connecting the cells in series and parallel [24]. The hottest debate in the electric power industry has been introduced about which battery technology will be the ultimate winner.

Many different types of batteries have been considered and developed for electric power system over the last years, such as: lead acid, nickel–cadmium (Ni–Cd), nickel–metal hydride (Ni–MH), and lithium-ion (Li-ion) [25,26]. This last one has the best characteristics with high voltage, light mass, low self-discharge, more lifetime and other advantages [27]. For these reasons, the Li-ion has been selected as the most favorable technology because it well matches the required characteristics [26,28].

3.7.2. Li-ion battery model

In this paper, a battery model based a simple nonlinear equivalent circuit is used. The structure did not model the internal chemistry of the Li-ion battery directly; the equivalent circuit empirically approximated the behavior seen at the battery terminals. The structure consisted of two main parts: a main branch which approximated the battery dynamics under most conditions, and a parasitic branch which accounted for the battery behavior at the end of a charge [29]. Fig. 5 illustrates the proposed model. However, this model assumes the same characteristics for the charge and the discharge cycles. The open voltage source is calculated with a non-linear equation based on the actual state of charge (SOC) of the battery [29,30].

E	no-load voltage (V)
E_0	battery constant voltage (V)
K	polarization voltage (V)
Q	battery capacity (Ah)
$\int idt$	actual battery charge (Ah)
A	exponential zone amplitude (V)
B	exponential zone time constant inverse $(\text{Ah})^{-1}$
V_{bat}	battery voltage (V)
R_{int}	internal resistance (Ω)
i	battery current (A)

The Li-ion battery model was designed with current like input and the voltage, SOC as variables outputs. This model does not take into account the influence of temperature and the phenomenon of self-discharge [30]. Under validate our battery model; we carry out a constant current test. Fig. 6 shows the battery voltage in discharge phase with constant current ($I_{bat} = 16$ A).

4. Control of the WECS in isolated mode

4.1. DFIG control

The originality of this control strategy lies in the choice of the rotor-flux components for a vector control, the rotor-flux is a natural state vector of the DFIG, and furthermore it allows a direct control over the rotor-voltage of the machine compared to a rotor-current inner loop method [8,14].

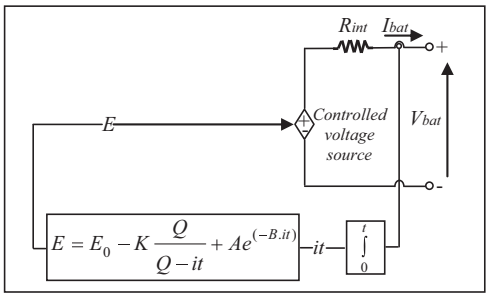

Fig. 5. Non-linear battery model [30].

The control strategy (Fig. 7a) is realized through two loops: an inner rotor flux control loop and an outer stator voltage loop where stator-voltage magnitude is regulated to follow the desired reference [15].

The DFIG stator voltage frequency is regulated by using the classical frequency relationship of the induction machine:

$$\omega_s = \omega_r + p\Omega \tag{34}$$

The rotor angular frequency ω_r changes according to the variable mechanical speed for regulating the stator angular frequency ω_s.

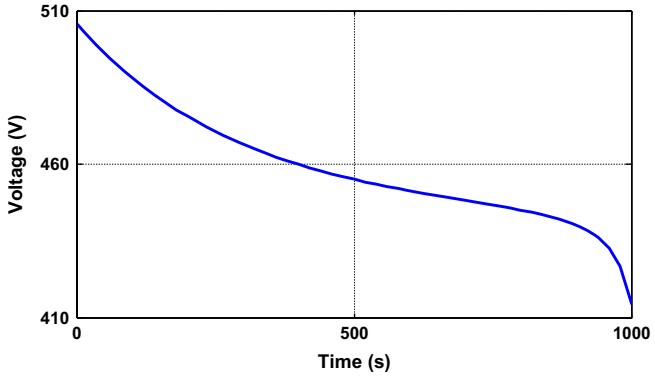

Fig. 6. Battery voltage with constant current.

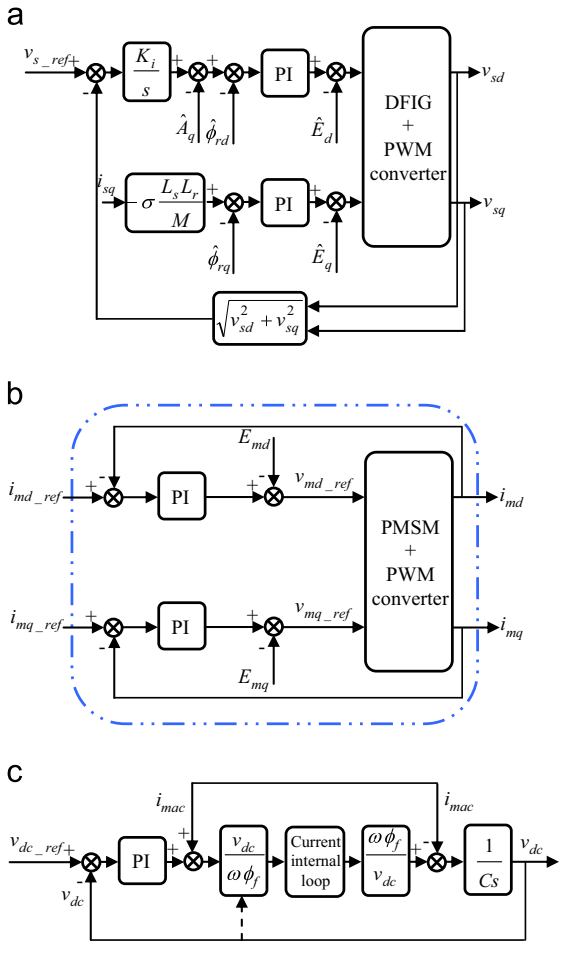

Fig. 7. Control strategies of the DFIG and PMSM. (a) Control strategy of DFIG. (b) Internal control loop of PMSM current. (c) External control loop of DC bus voltage.

4.1.1. Rotor-flux inner loop

In order to impose the rotor current dynamic and to control the stator voltage via the rotor flux, a simple PI controller is employed.

4.1.2. Stator-voltage outer loop

The voltage control loop is used to control the magnitude of the stator voltage spatial-vector, which is defined as follows:

$$|v_s| = \sqrt{v_{sd}^2 + v_{sq}^2} \tag{35}$$

where $|v_s|$ is the stator voltage vector magnitude. The voltage control loop is closed by using the voltage magnitude, as calculated in (35).

The transfer function between stator voltage and rotor flux is a simple gain, thus a simple integrator is used for the regulation to cancel the static error between measured and reference stator voltage (Fig. 7a).

4.2. PMSM control

In order to regulate the dc bus voltage independent of the rotor power of DFIG using PWM converter with PMSM, we need two control loops [8,15].

- Internal loop current control of PMSM
- External control loop of the dc bus voltage

The two control loops are shown in Fig. 7.

4.3. Storage system control

The management strategy is used to control the energy storage in the Li-ion battery storage system. It is designed to smooth wind power fluctuations by releasing or absorbing stored energy during wind fluctuations [17,18,23]. It is well known that the wind speed is fluctuant and, because of this, the wind generator delivers a variable electrical power. To overcome this drawback, a Li-ion battery storage system is installed in order to produce an additional energy and regulate the electric power delivered to the isolated grid [18]. The reference active power applied to the Li-ion battery storage is obtained by the following equation:

$$P_{bat} = P_{load} - P_{wind} \tag{36}$$

where P_{load} the reference load active power, fixed to 7.5 kW value and P_{wind} is the power generated by the DFIG.

5. Simulation results

In order to verify the performance of the proposed wind energy conversion system for stand-alone power applications, the simulation work has been done by using Matlab/Simulink package. The parameters of the simulation studies are listed in the Appendix. Several tests were performed with the result interpretation. However, some results of these tests are presented in this section.

Fig. 8 illustrates the DFIG mechanical speed profile. This profile is chosen to show the DFIG behavior in sub synchronous and hyper synchronous as well.

Fig. 9a displays the simulation waveform of the d,q components of DFIG stator voltage output while Fig. 9b illustrates the instantaneous first phase stator voltage and current.

It is clearly shown from Fig. 9b that the stator voltage follow its reference set in this case at $220\sqrt{2}$ V and frequency of 50 Hz during a change of mechanical speed and the stator current is in phase with the voltage (resistive load).

Fig. 10a and b presents the power of wind turbine, load and battery in our system. It is noticed that during the transition from

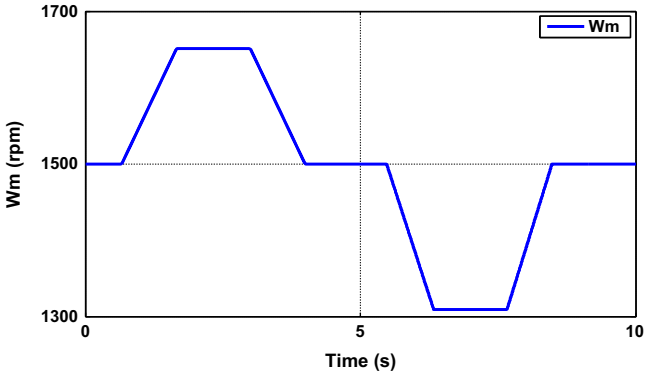

Fig. 8. Mechanical speed profile.

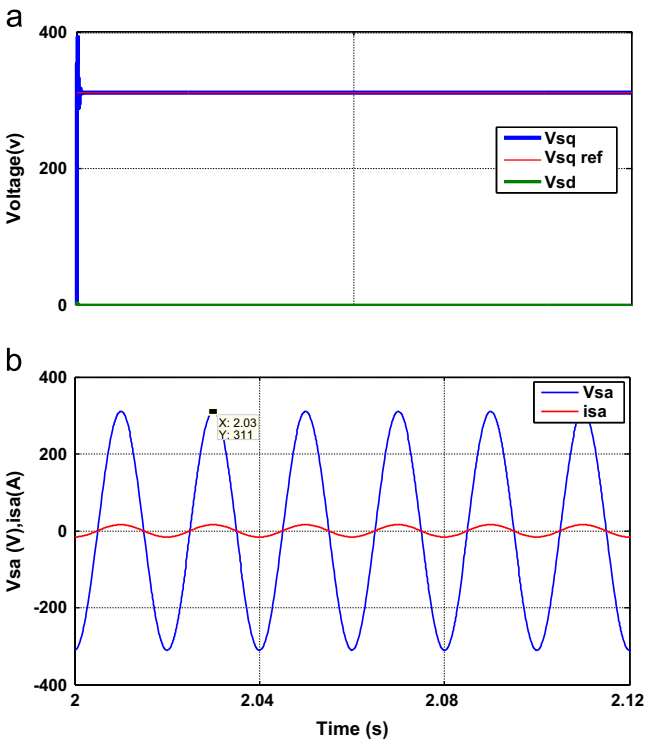

Fig. 9. Simulation waveforms of the DFIG stator voltage output. (a) d and q components of the DFIG stator voltage. (b) The stator voltage and current.

the synchronous mode to the hyper synchronous mode the wind power change between load power value and max value, this deference is recovered by Li-ion battery storage system. On the other hand, the battery ensures the power gap between the wind turbine and load demand in low speed range.

From Fig. 10a and b, we can distinguish three operation modes of our system:

- First mode: the wind power equal to the power demand of load, we can see that the Li-ion battery storage system is not operated during this phase.
- Second mode: the value of wind power is greater than the load demand. So, the power gap in this range is recovered by the Li-ion battery storage system.
- Third mode: the wind power is less than the power need of load in this phase. However, the Li-ion battery storage system ensures the power gap between the wind turbine and load demand.

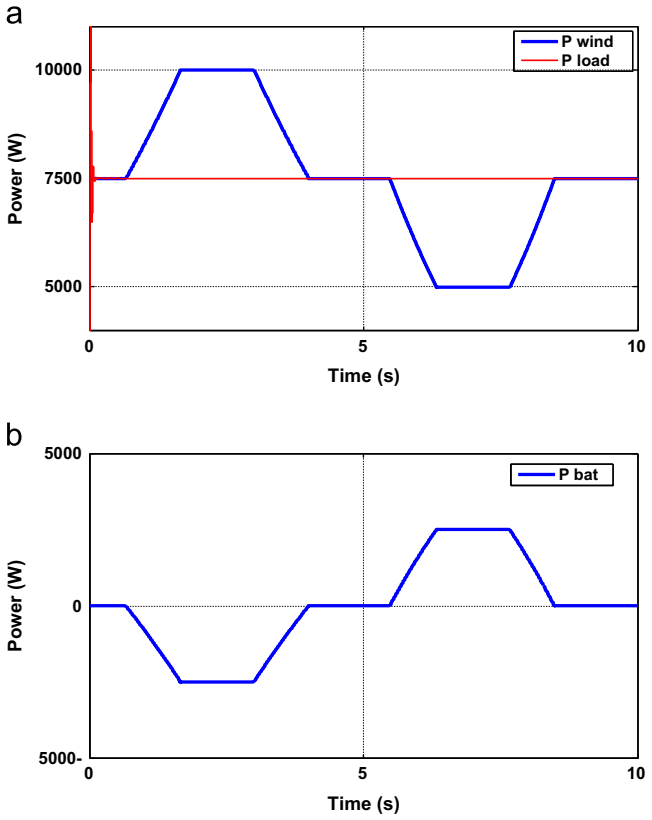

Fig. 10. Simulation waveforms of the WECS power. (a) Wind and load power. (b) Battery power.

Fig. 11 illustrates the variation of battery voltage during the change of power cycle. The charging and discharging of the battery is according the power demand.

The determination of the battery SOC is very important for the proposed wind energy conversion system for stand-alone power applications. Fig. 12 presents the SOC given by the Li-ion battery with both operation mode charging and discharging (initially charged with 80%).

We can see from Figs. 10, 11 and 12 the Li-ion battery storage system work in the main phases during the operation of proposed system. These results confirm the need of storage system in our installation to provide an isolated load through a stand-alone wind power system.

Fig. 13 presents the dc bus voltage; we can see that the dc bus voltage reaches its reference value with good approximation even during changes of mechanical speed. This result confirms the feasibility of the proposed PMSM control.

In order to evaluate the robustness of proposed system under load variation, a simulation test is carried out (Fig. 14), which the mechanical speed of wind turbine is kept at 1500 rpm and the resistive load is reduced to the half,in the same time a reactive load is connected to wind power supply. Fig. 14a shows that our system is able to provide the necessary power for the load before and after the change ($t=5$ s). We can see also a small delay in the curve of battery power during the load variation, which related to the time constant of both battery and dc/dc converter.

Fig. 14b illustrates the decrease of battery voltage with a time gap during load change. This discharging of battery is affected to ensure the load power demand.

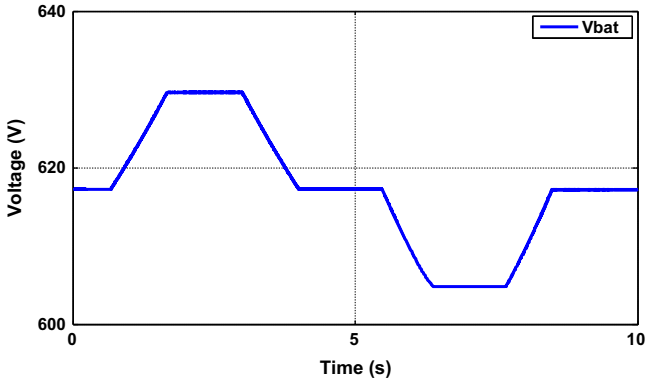

Fig. 11. Battery voltage waveform.

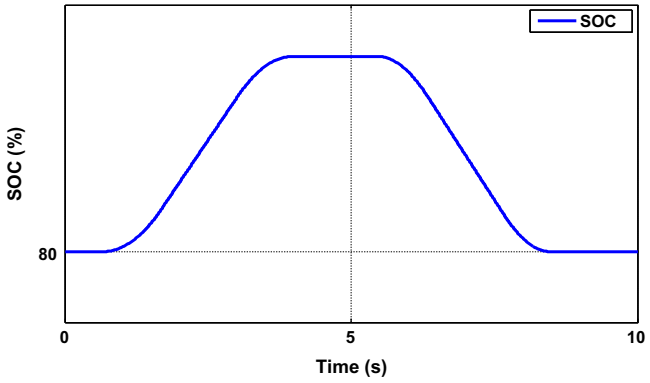

Fig. 12. State of charge (SOC).

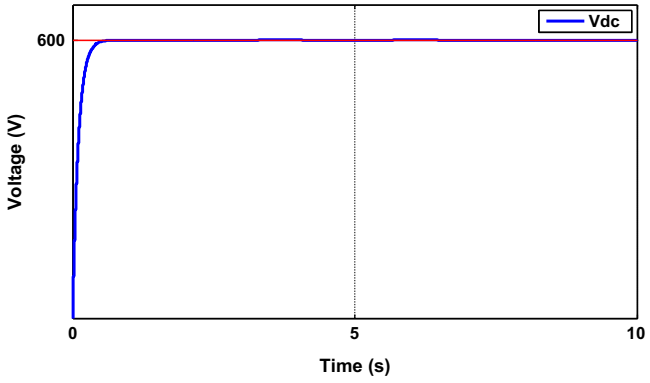

Fig. 13. Dc bus voltage.

The stator voltage and current are shown in Fig. 14c, it is clearly shown that the both DFIG stator voltage magnitude and frequency are kept constant during all operation phases. As well as, we can see from the same figure that after change time a difference in the phase between DFIG stator voltage and current due to new reactive load connected in wind power supply. However, this result confirm that our system can be provides both reactive and active powers under different conditions.

Another test is realized to confirm the good performances of our system in stand-alone power applications (Fig. 15). The test is consisting to keep the resistive load at a constant value with decreasing the mechanical speed of wind turbine to low value 500 rpm (Fig. 15a). As Fig. 15b shows, the load power is always

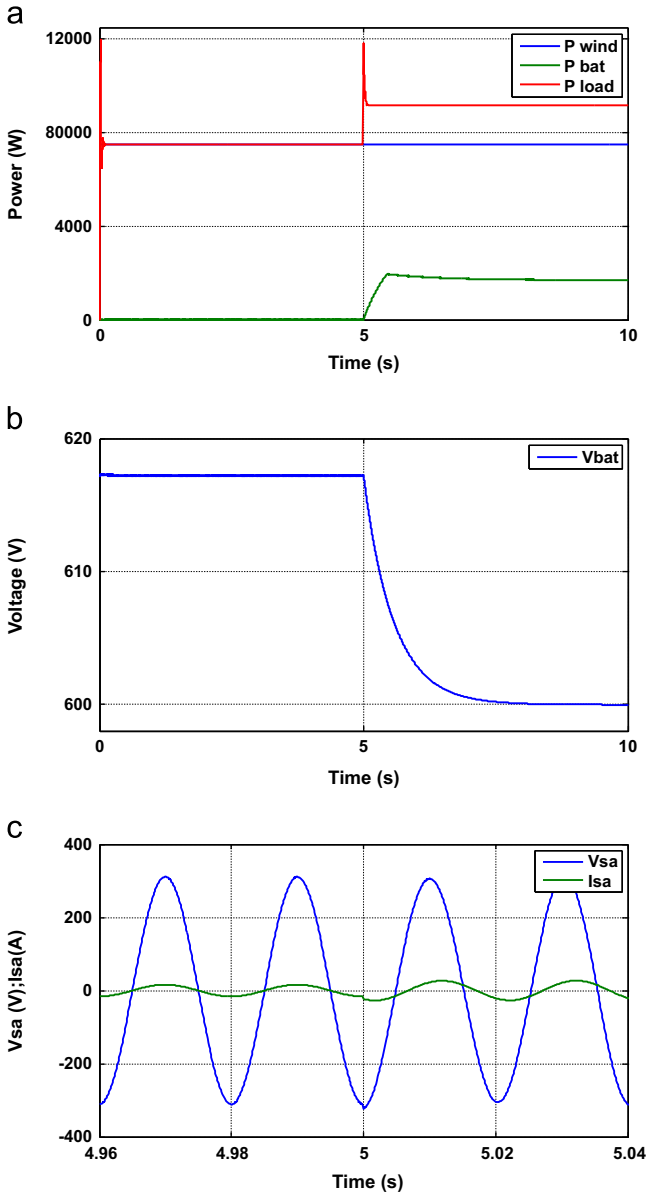

Fig. 14. Test of load variation with constant speed (1500 rpm). (a) Wind, battery and load powers. (b) Battery voltage waveform (c) DFIG stator voltage and current.

assured by wind power supply even under lower speed. The power battery increases only to compensate the deference between the wind power and load. Fig. 15c presents that the magnitude and frequency of DFIG stator voltage are well controlled, which there is not any influences of wind speed on our system.

Based on this study, we can say that the proposed stand-alone wind power system offer many advantages in comparison with the traditional wind supply. The use of tow machines DFIG and PMSM in the same system allow to decrease the power stress applied to Li-ion battery storage system and optimize the size of both battery pack and PMSM, as well as the power converters. In addition, the good performances and high yield of proposed system is confirmed by simulation tests, when the ability of power supply to provide an isolated load during wind speed variation and under load change. Nevertheless, the drawback of stand-alone wind power system is high cost and its problem is lifetime of the Li-ion battery storage system. More than that, the coupling of tow electric machines in the same turbine with dissimilar power can created a mechanical problems and generate more noise.

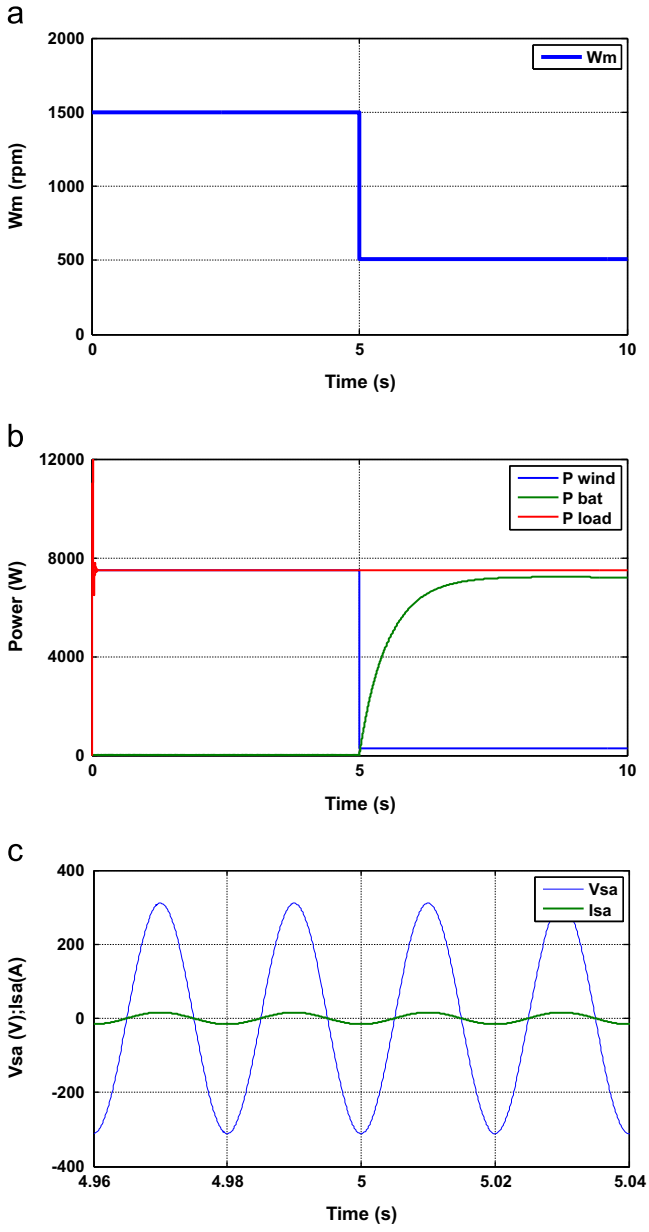

Fig. 15. Test in phase of low wind speed. (a) Mechanical speed profile. (b)Wind, battery and load powers. (c) DFIG stator voltage and current.

6. Conclusions

In this paper, a structure of stand-alone wind power system based on a DFIG and PMSM associated with Li-ion battery storage system was presented. In addition, a control strategy for the stand-alone DFIG was developed to regulate the DFIG stator voltage magnitude and frequency. This strategy uses the d and q components control of rotor flux. The PMSM is connected to the rotor of the generator via the back-to-back PWM converter. It is controlled to somehow to keep the dc link voltage magnitude constant under variable mechanical speed operation. However, the energy management strategy for storage system is selected to smooth wind power fluctuations using the Li-ion battery. According to the simulation results presented the proposed stand-alone wind power system have the ability to cover the corresponding load demand in both hyper synchronous and sub synchronous mode. Finally, the capacity of the battery and energy management strategy used in wind based stand-alone installation are very important factors for the feasibility and effectiveness of our system.

Appendix

DFIG parameters	$P_{DFIG} = 7.5$ kW $R_s = 0.455\ \Omega$ $R_r = 0.455\ \Omega$ $L_s = 84$ mH $L_r = 81$ mH $M = 78$ mH $p = 2$ $f = 0.00673$ Nm/s $\sigma = 0.0106$ $J = 0.3125$ kg m^2
PMSM parameters	$P_{PMSM} = 5.1$KW $R_{ms} = 2.43\ \Omega$ $L_d = 30.6$ mH $L_q = 29.1$ mH $P = 5$ $K_e = 194$ $k_m = 0.16$ $J = 0.0035$ kg m^2
Li-ion battery parameters	$Q = 1.5$ Ah $R_{int} = 0.02\ \Omega$ $E_0 = 1.2449$ V $K = 0.0029221$ V $A = 0.156$ V $B = 2.35\ 29\ (\text{Ah})^{-1}$ N = 120 M = 2

References

[1] Kaldellis JK, Kavadias KA, Koronakis PS. Comparing wind and photovoltaic stand-alone power systems used for the electrification of remote consumers. Renew Sustainable Energy Rev 2007;11:57–77.
[2] Alnasir Z, Kazerani M. An analytical literature review of stand-alone wind energy conversion systems from generator viewpoint. Renew Sustainable Energy Rev 2013;28:597–615.
[3] Fadaeenejad M, Radzi MAM, Abkadir MZA, Hizam H. Assessment of hybrid renewable power sources for rural electrification in Malaysia. Renew Sustainable Energy Rev 2014;30:299–305.
[4] Kaundinya DP, Balachandra P, Ravindranath NH. Grid-connected versus stand-alone energy systems for decentralized power—a review of literature. Renew Sustainable Energy Rev 2009;13:2041–50.
[5] Sinha S, Chandel SS. Review of software tools for hybrid renewable energy systems. Renew Sustainable Energy Rev 2014;32:192–205.
[6] Patin N, Monmasson E, Louis JP. Analysis and control of a cascaded doubly-fed induction generator. In: Proceedings of the 31st Annual Conference of the IEEE Industrial Electronics Society, IECON'05; 2005. p. 2487–92.
[7] Hopfensperger B, Atkinson DJ, Lakin RA. Combined magnetising flux oriented control of the cascaded doubly-fed induction machine. In: Proceeding of Electric Power Applications; 2001. p. 354–62.
[8] Khatounian F, Monmasson E, Berthereau F, Delaleau E, Louis JP. Control of a doubly fed induction generator for aircraft application. In: Proceeding of the IEEE IECON'03; 2003. p. 2711–16.
[9] Khahro SF, Tabbassum K, Soomro AM, Liao X, Alvi MB, Dong L, et al. Techno-economical evaluation of wind energy potential and analysis of power generation from wind at Gharo, Sindh Pakistan. Renew Sustainable Energy Rev 2014;35:460–74.
[10] Zeng R, Nian H, Quan Y, Liu J. Improved load-adaptive control strategy for PMSG based stand-alone wind energy generation system. In: Proceeding of the International Conference on Electrical Machines and Systems, ICEMS'09; 2009. p.1–6.
[11] Serra FM, De Angelo CH, Forchetti DG. Passivity-based control of a three-phase front end converter for stand alone wind generation system. In: Proceeding of

the 10th IEEE/IAS International Conference on Industrial Applications, INDUSCON'12;. 2012. p. 1–5.
[12] Wang C, Li J, Colson CM, Nehrir MH. Power management of a stand-alone hybrid wind-microturbine distributed generation system. In: Proceeding of the Power Electronics and Machines in Wind Applications, PEMWA'09; 2009. p. 1–7.
[13] Nguyen N, Lee H. An effective harmonic elimination for DFIG feeding non-linear loads in stand-alone operation. In: Proceeding of the 38th Annual Conference of the IEEE Industrial Electronics Society, IECON'12; 2012. p. 3527–32.
[14] Forchetti D, Garcia G, Valla MI. Vector control strategy for a doubly-fed stand-alone induction generator. In: Proceeding of the 28th Annual Conference of the IEEE Industrial Electronics Society, IECON'02; 2002. p. 991–5.
[15] Khatounian F, Monmasson E, Berthereau F, Louis JP. Design of an output LC filter for a doubly fed induction generator supplying non-linear loads for aircraft applications. In: Proceeding of the IEEE International Symposium on Industrial Electronics, ISIE'04; 2004. p. 1093–8.
[16] Ziogou C, Ipsakis D, Elmasides C, Stergiopoulos F, Papadopoulou S, Seferlis P, et al. Automation infrastructure and operation control strategy in a stand-alone power system based on renewable energy sources. J Power Sour 2011;196:9488–99.
[17] Ipsakis D, Voutetakis S, Seferlis P, Stergiopoulos F, Elmasides C. Power management strategies for a stand-alone power system using renewable energy sources and hydrogen storage. Int J Hydrogen Energy 2009;34:7081–95.
[18] Belfedhal SA, Berkouk EM, Meslem Y, Soufi Y. Modeling and control of wind power conversion system with a flywheel energy storage system and compensation of reactive power. Int J Renew Energy Res 2012;2:528–34.
[19] Mesbahi T, Ghennam T, Berkouk EM. Control of a wind energy conversion system with active filtering function. In: Proceeding of the International Conference on Power Engineering, Energy and Electrical Drives, POWERENG; 2011. p. 1–6.
[20] Ghennam T, Berkouk EM, Francois B. Modeling and control of a doubly fed induction generator (DFIG) based wind conversion system. In: Proceeding of the International Conference on Power Engineering, Energy and Electrical Drives, POWERENG'09; 2009. p. 507–12.
[21] Ghennam T, Berkouk EM, Francois B. DC-link voltage balancing algorithm using a space-vector hysteresis current control for three-level VSI applied for wind conversion system. In: Proceeding of the European Conference on Power Electronics and Applications, EPE'07; 2007. p. 1–10.
[22] Ghedamsi K, Aouzellag D, Berkouk EM. Control of wind generator associated to a flywheel energy storage system. Renew Energy 2008;33:2145–56.
[23] Mesbahi T, Ouari A, Ghennam T, Berkouk EM, Mesbahi. N. A hybrid wind energy conversion system/active filter for non linear conditions. Int J Syst Assur Eng Manag 2014, http://dx.doi.org/10.1007/s13198-014-0250-5, in press.
[24] Divya KC, Østergaard J. Battery energy storage technology for power systems—an overview. Electr Power Syst Res 2009;79:511–20.
[25] Benson CL, Magee CL. On improvement rates for renewable energy technologies: solar PV, wind turbines, capacitors, and batteries. Renew Energy 2014;68:745–51.
[26] Merei G, Berger C, Sauer DU. Optimization of an off-grid hybrid PV–Wind–Diesel system with different battery technologies using genetic algorithm. Sol Energy 2013;97:460–73.
[27] Miranda ÁG, Hong CW. Integrated modeling for the cyclic behavior of high power Li-ion batteries under extended operating conditions. Appl Energy 2013;111:681–9.
[28] Świerczynski M, Stroe DI, Stan AI, Teodorescu R, Sauer DU. Selection and performance-degradation modeling of $LiMO_2/Li_4Ti_5O_{12}$ and $LiFePO_4$/C battery cells as suitable energy storage systems for grid integration with wind power plants: an example for the primary frequency regulation service. IEEE Trans Sustainable Energy 2014;5:90–101.
[29] Tremblay O, Dessaint LA, Dekkiche AI. A generic battery model for the dynamic simulation of hybrid electric vehicles. In: Proceeding of the IEEE Vehicle Power and Propulsion Conference, VPPC'07; 2007. p. 284–9.
[30] Mesbahi T, Rizoug N, Bartholomeus P, Le Moigne P. Li-ion battery emulator for electric vehicle applications. In: Proceeding of the IEEE Vehicle Power and Propulsion Conference, VPPC'13; 2013. p. 191–8.